Development of a Computationally Efficient, High Fidelity, Finite Element Based Hall Thruster Model

Subrata Roy
Computational Plasma Dynamics Laboratory
Kettering University
1700 West Third Avenue
Flint, MI 48504

This report documents the development of a two dimensional finite element based numerical model for efficient characterization of the Hall thruster plasma dynamics in the framework of multi-fluid model. Effect of the ionization and the recombination has been included in the present model. Based on the experimental data, a third order polynomial in electron temperature is used to calculate the ionization rate. The neutral dynamics is included only through the neutral continuity equation in the presence of a uniform neutral flow. The electrons are modeled as magnetized and hot, whereas ions are assumed unmagnetized and cold. The dynamics of Hall thruster is also investigated in the presence of plasma-wall interaction. The plasma-wall interaction is a function of wall potential, which in turn is determined by the secondary electron emission and sputtering yield. The effect of secondary electron emission and sputter yield has been considered simultaneously. Simulation results are interpreted in the light of experimental observations and available numerical solutions in the literature.

Nomenclature:

B, $\mathbf{B}$	Magnetic field, gauss
E	Electron charge, coulomb
E_i	Ionization potential, eV
E, $\mathbf{E}$	Electric field, V/m
j, J	Current, mA
L	Differential operator
M	Mass, kg
$\mathbf{M}$	Mass matrix
N	Number density, m^{-3}
N	Basis function
R	Radial direction
$\mathbf{R}$	Solution residual
S	Assembly operator
T	Time, s
T	Temperature, eV
U, $\mathbf{U}$	State variable
V, $\mathbf{V}$	Velocity, m/s

w	Weight function
Xe	Xenon
Z	Axial direction
Z	Ionicity

Greek

ν	Collision frequency, s^{-1}
ϕ	Potential, volt
Γ	Flux of the propellant, m^{-2}s^{-1}
Ω	Solution domain
σ	Ionization cross-section, m^2
ϑ	Implicitness
Δ	Step

Subscripts

$*, 0$	Reference value
C	Charge exchange
D	Discharge
e	Electron
i	Ion
k	Degree of interpolation polynomial
H	Hall current
n	Neutrals
r	Radial component
t	Thermal velocity
z	Axial component
α	Electron or ion
θ	Azimuthal component
τ	Time stepping index

Superscript

s	
h	Discretization
p	Iteration index
0	Neutrals
$+$	Singly ionized
$++$	Doubly ionized

I. Introduction

Hall effect thruster (HET) is a highly effective on-board propulsion device popular in many LEO and GEO satellites.[1] It is also called "closed drift" thruster (CDT) due to the azimuthal drift of electrons.

This is common to variants of such thrusters, e.g. stationary plasma thruster (SPT), thruster with anode layer (TAL) etc. The SPT thruster is a coaxial device that consists of four main parts: the anode, which serves as a propellant distributor; an annular acceleration channel made of boron nitride; a magnetic unit; and a hollow cathode (Fig. 1). The plasma column is contained within two coaxial dielectric cylinders that constitute the discharge channel, with the anode at one end of the channel and the exit at the other end of the channel. The discharge is created between the anode of the thruster and an external hollow cathode located downstream of the channel exit. The magnetic system consists of a series of electromagnetic coils employed inside the inner cylinder and outside the outer cylinder, and predominantly radial field with a maximum just upstream of the channel exit. The electrons from the cathode enter the chamber and are subject to azimuthal $\mathbf{E} \times \mathbf{B}$ drift. The electrons in the closed drift undergo ionizing collisions with the propellant gas. While the magnetic field is strong enough to capture electrons in an azimuthal drift, it is not strong enough to contain the resulting ions, which are essentially accelerated by the imposed axial electric field. The suppression of axial electron mobility by the imposed radial magnetic field, while leaving ion mobility unaffected, enables the plasma to support an electric field with a potential difference close to the applied voltage. The ions are accelerated to kinetic energies within 80% of the applied discharge voltage.[2]
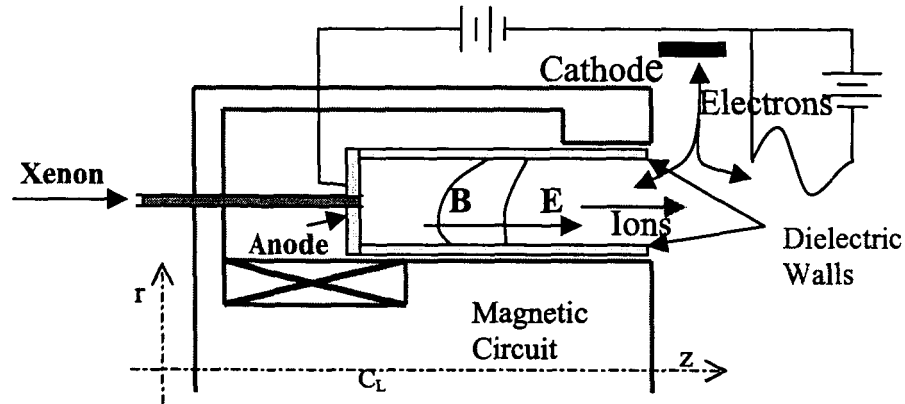

Figure 1. Half-plane schematic of a single stage stationary plasma thruster.

Present day Hall thrusters offer specific impulses over 2400 s, thrust over 1 N, and power exceeding 50 kW at efficiencies close to 60%.[3] However, the commercial exploitation of Hall thrusters imposes a stringent constraint of trouble free operation for more than 8000 hrs.[4] The physics inside the Hall thruster has to be reasonably well understood in order to make any significant change in efficiency without compromising the lifetime. This is a challenge, as the choice of thruster size requires an optimum selection between efficiency and lifetime.[5] Despite significant numerical and theoretical advances of the recent past, we lack an adequate numerical model to describe critical regions of a Hall thruster plasma dynamics in a self-consistent fashion.[6-7] This effort was focused towards developing a consistent formulation for practical SPT simulation.

Numerical simulation of the plasma dynamics of a Hall thruster has been carried out recently by several authors in the framework of the hybrid as well as the fluid models.[8-28] The one-dimensional (1D) fluid model of the partially ionized plasma incorporating the neutral dynamics and the effect of the plasma-wall interaction has been documented recently.[26-28] This report presents the numerical and theoretical

development a 2D, three-fluid, partially ionized plasma model in order to investigate the effect of ionization and recombination on the dynamics of the Hall thruster. The neutral dynamics is included in the present work since without neutral dynamics the effect of ionization and recombination cannot be studied satisfactorily. The self-consistent 2D, three-fluid formulation of the bounded thruster plasma is the novel feature of this report. To the best of our knowledge, such a simulation has not been reported in the literature.

Numerical novelty includes the utilization of sub-grid embedded (SGM) finite elements,[29-30] for convergence and stability of the solution. It is based on a non-linear, non-hierarchical, high-degree Lagrange finite element basis for use in a discretized approximation. SGM elements utilize local mesh, velocity and diffusion parameters to modify the dissipative flux vector (second derivative) terms in the equation. For the hyperbolic equation, a second derivative artificial diffusion term with a vanishing coefficient is added. The theory employs element-level static condensation and eigenvalue analysis for efficiency, nodal-rank homogeneity and essentially non-oscillatory solution. Unlike traditional upwind methods, however, non-linear SGM does not introduce any unnecessary diffusion to distort the solution.

The numerical model and the simulation results are presented in the subsequent sections. In section II, we discuss pertinent theoretical issues. In section III, the solution algorithm is described. The numerical results are documented in section IV. Finally, section V contains conclusions and future work.

II. Theoretical Issues
The dynamics of a partially ionized, thruster plasma is quite complicated,[1-4,8-13,16,18-21,27,28] as several elastic and inelastic processes may occur simultaneously. However, not all processes are equally probable. For example, momentum exchange between electron-electron and ion-ion will not be important in comparison with the electron-ion momentum exchange as the relative drift between similar particles is small in comparison with the drift between electrons and ions. The collisions between electron-neutral, electron-ion, and ion-neutral play an important role. The plasma-neutral collision usually determines the kinetics of the motion.

(a) Ionization: Electrons collision with the neutral atom is the main source of ion production in propulsion plasma. The rate of ion production in plasma is determined by the total cross section of the process.

$$S_{ioniz} = n_e n_n \langle V \sigma^i(V) \rangle = k_{en}^i n_e n_n \qquad (6)$$

where, for *process constant* $k^i = \langle V \sigma^i(V) \rangle$, the averaging is done over the velocities of the electrons whose energy is sufficient for ionization $mV^2/2 > E_i$. The ionization source term, which takes into account all the above processes, is

$$S_{ionization} = k_i^{0+} n_e n_n + k_i^{0++} n_e n_n + k_i^{1++} n_e^2 \qquad (7)$$

where 0+, 0++ represents the transition from neutral to singly and doubly ionized state respectively ($Xe^0 \rightarrow Xe^+$ and $Xe^0 \rightarrow Xe^{++}$) and 1++ represents the transition from singly to doubly ionized state

4

($Xe^+ \rightarrow Xe^{++}$). A general third order temperature dependant polynomial can be fitted to the experimental value of ionization rate $k_i = k_i^{0+} + k_i^{0++} + k_i^{1+}$. The matrix form is

$$\begin{pmatrix} k_i^{0+} \\ k_i^{0++} \\ k_i^{1++} \end{pmatrix} = \begin{pmatrix} 1.9435\times10^{-5} & -0.0068 & 0.6705 & -1.6329 \\ -3.0352\times10^{-5} & 0.0024 & 0.0515 & -0.1431 \\ -2.117\times10^{-5} & 0.0022 & -0.0119 & 0.0161 \end{pmatrix} \begin{pmatrix} T_e^3 \\ T_e^2 \\ T_e^1 \\ T_e^0 \end{pmatrix} \times10^{-14} \quad (8)$$

The sum of all three ionization rates can be represented as,

$$k_i = (-3.2087\times10^{-5}T_e^3 - 0.0022T_e^2 + 0.7101T_e - 1.76)\times10^{-14} \quad (9).$$

Above estimate of ionization rate is based on the Maxwellian distribution function.

(b) Recombination: The plasma-wall interaction leads to the recombination of the plasma particles at the wall. Furthermore, the recombination in the presence of a neutral body (wall) is important at the low degree of ionization. The *recombination coefficient* α can be approximated as[31] $\alpha = 1.09\times10^{-20}\, n_e\, T^{-9/2}\, m^3/s$. Then the recombination rate can be written as $S_{recom} = -1.09\times10^{-20}\, T^{-9/2}n_e^3\, m^3/s$, where assuming quasi-neutrality n_i has been replaced by n_e.

(c) Charge-exchange process: Charge exchange is related with the transfer of one or more electrons between an atom and an ion. Slow propellant ions are created due to resonant charge-exchange collisions between the fast "beam" (current) ions and slow thermal neutrals. The spatial volumetric production rate is given by $S_{CEX} = n_n n_i \langle v_i \sigma(v_i) \rangle$, where relative collision velocity is taken to be the ion velocity.

$Xe_{fast}^+ + Xe_{slow}^0 \rightarrow Xe_{slow}^+ + Xe_{fast}^0$, $Xe_{fast}^{++} + Xe_{slow}^0 \rightarrow Xe_{slow}^{++} + Xe_{fast}^0$, $Xe_{fast}^{++} + Xe_{slow}^0 \rightarrow Xe_{slow}^+ + Xe_{fast}^+$.

The process can be important for creating slow ions. The collisional cross-section for the above processes are comparable[31] $\sigma(Xe - Xe^+) \sim 4.38\times10^{-19}\, m^2$ and $\sigma(Xe - Xe^{++}) \sim 4.98\times10^{-19}\, m^2$. Thus, it would appear that all the above processes are equally important. However, in the last process stripping of an electron may require energy exceeding 1 keV[33] and thus, the last process is ignored. The cross section for Xe-Xe^+ for example is given by[34]

$$\sigma(Xe - Xe^+) = \left[a - b\log_{10}(\Delta u)\right]\left(E_i/E_H\right)^{-1.5}\times10^{-20}\,m^2. \quad (9)$$

where $a = 181$, $b = 21.2$, $E_i = 12.13$ eV - xenon ionization potential and $E_H = 13.6$ eV - hydrogen ionization potential. For a relative velocity Δu between 10 and 2×10^3 m/s, the charge exchange cross-section varies between 10^{-20} to $10^{-19}\, m^2$.

Having delineated some of the important physical processes in the partially ionized thruster plasma, we shall now give the basic set of equations that describes the dynamics of the process under investigation. We shall assume that the ions are unmagnetized, since for typical parameters of a thruster plasma viz., magnetic field B ~ 200G and ion velocity 4×10^3 m/s the gyration radius of ions are about 0.1 m, which is much larger than the size of the thruster (0.02 – 0.03 m). In the present simulation, the maximum

value of magnetic field, near the exit, is 242 G. Therefore, the effect of magnetic field on the ion transport will be ignored. Further, the pressure term in the ion momentum equation can be ignored as the thermal energy of the ions is much smaller than their kinetic energy i.e. $T_i << m_i V_i^2$. Note that owing to the small inertia, electron response time is much faster than the ion response time. As a result, electrons will attain the steady state faster than the ions. Keeping this in mind, electron momentum and energy equations are solved at steady state, whereas for ions and neutrals, a set of time-dependent continuity and momentum equations are simultaneously solved.

An annular cylinder can adequately characterize Hall thruster geometry. Ignoring any variation in the azimuthal (θ) direction, we shall take a two-dimensional axisymmetric (r, z) representation of the thruster. The following set of equations written in the component form is used to describe the dynamics of thruster plasma with the azimuthal ion velocity, $V_{i\theta}$, and dependence on the azimuthal angle, $\partial/\partial\theta$, set to zero. The continuity equation for the electron and the ions are,

$$\frac{\partial n_a}{\partial t} + \frac{1}{r}\frac{\partial}{\partial r}(r\, n_a V_{ar}) + \frac{\partial(n_a V_{az})}{\partial z} = S, \qquad (6)$$

where $S = S_{recomb} + S_{ioniz} + S_{cex}$. Assuming that the neutral velocity has axial component only, the neutral continuity equation is

$$\frac{\partial n_n}{\partial t} + \frac{\partial(n_n V_{nz})}{\partial z} = S_{recomb} - k_i^{0+} n_e n_n - k_i^{0++} n_e n_n. \qquad (7)$$

The right hand side of the continuity equations (6)-(7) represents source and sink term due to ionization and recombination. The sink term of the neutral continuity equation (7) is slightly different than the ionization source term of the plasma continuity equation (6) due to the presence of the processes like $Xe^+ \rightarrow Xe^{++}$ in the S_{ioniz}.

The ion momentum equations are,

$$\frac{\partial V_{ir}}{\partial t} + V_{ir}\frac{\partial V_{ir}}{\partial r} + V_{iz}\frac{\partial V_{ir}}{\partial r} = -\frac{T_i}{m_i n_i}\frac{\partial n_i}{\partial r} + \left(\frac{Ze}{m_i}\right)E_r - v_c V_{ir} + \left(\frac{m_e}{m_i}\right)v_{ei}(V_{er} - V_{ir})$$
$$-0.5\, v_{in}(V_{ir} - V_{nr}) + \left(\frac{S}{n_i}\right)V_{ir}\,, \qquad (8)$$

$$\frac{\partial V_{iz}}{\partial t} + V_{ir}\frac{\partial V_{iz}}{\partial r} + V_{iz}\frac{\partial V_{iz}}{\partial z} = -\frac{T_i}{m_i n_i}\frac{\partial n_i}{\partial z} + \left(\frac{Ze}{m_i}\right)E_z - v_c V_{iz} + \left(\frac{m_e}{m_i}\right)v_{ei}(V_{ez} - V_{iz})$$
$$-0.5\, v_{in}(V_{iz} - V_{nz}) + \left(\frac{S}{n_i}\right)V_{iz}. \qquad (9)$$

The factor 0.5 before ion-neutral collision term comes from reduced mass $m_i m_n /(m_i+m_n) \approx m_i/2$.

The electron momentum equations are,

$$V_{er}\frac{\partial V_{er}}{\partial r} + V_{ez}\frac{\partial V_{er}}{\partial z} - \frac{V_\theta^2}{r} = -\frac{1}{m_e n_e}\frac{\partial n_e T_e}{\partial r} - \frac{e}{m_e}(E_r + V_{e\theta}B_z) - v_{ei}(V_{er} - V_{ir}) - v_{en}(V_{er} - V_{nr}) + \left(\frac{S}{n_e}\right)V_{er}, \qquad (10)$$

$$V_{er}\frac{\partial V_{e\theta}}{\partial r} + V_{ez}\frac{\partial V_{e\theta}}{\partial z} + \frac{V_{er}V_{e\theta}}{r} = -\frac{e}{m_e}(V_{ez}B_r - V_{er}B_z) + \left(\frac{S}{n_e}\right)V_{e\theta} - (v_{ei} + v_{en})V_{e\theta}, \qquad (11)$$

6

$$V_{er}\frac{\partial V_{ez}}{\partial r}+V_{ez}\frac{\partial V_{ez}}{\partial z}=-\frac{1}{mn_e}\frac{\partial n_eT_e}{\partial z}-\frac{e}{m_t}\left(E_z-V_{e\theta}B_r\right)-v_{ei}(V_{ez}-V_{iz})-v_{en}(V_{ez}-V_{nz})+\left(\frac{S}{n_e}\right)V_{ez} \tag{12}$$

The electron energy equation is,

$$\frac{3}{2}\left(\frac{\partial T_e}{\partial t}+\mathbf{V}_e\bullet\nabla T_e\right)=-T_e\nabla\bullet\mathbf{V}_e-v\left[V_{er}^2+V_{e\theta}^2+V_{ez}^2+2\left(V_{er}\left(V_{e\theta}+V_{ez}\right)+V_{ez}V_{e\theta}\right)\right]$$

$$+v_{ei}\left(V_{er}V_{ir}+V_{ez}V_{iz}\right)+v_{en}\left(V_{er}V_{nr}+V_{ez}V_{nz}\right)+3\frac{m_e}{m_i}v_{ei}(T_i-T_e)+3\frac{m_e}{m_n}v_{en}(T_n-T_e)+\frac{S}{n_e}\left(\frac{3}{2}T_e+\alpha E_i\right). \tag{13}$$

where $v=v_{ei}+v_{en}$. In equations (6)-(13), V_e, V_i are the electron and ion velocities, respectively. **E** and **B** are the electric and magnetic fields, and n_j is the number density of the j-th particle with $j=e$ and i, v_{ei}, v_{en} are the electron-ion and electron-neutral collision frequencies respectively, v_c is the ion charge-exchange collision frequency, e is the electron charge, Z is the ionicity, and the value of α is between (2 –3).[19] The electron dynamics are determined by the pressure gradient, electric and magnetic forces, and the collisional exchange of momentum in equations (10)-(12). The convective term in these equations retains the effect of the electron inertia.

The contribution of the electron inertia is small and on this basis, its effect on the plasma dynamics is generally ignored. However, in the regions of sharp flow gradients, the effect of the convective term may become finite, and therefore the convective term is retained in this formulation. Similarly, since collision time scales are much slower than the electron-cyclotron gyration time scale, one may ignore elastic and inelastic collision terms in comparison with the Lorentz force term $\mathbf{V}\times\mathbf{B}$ in the momentum equation. Such an approach will exclude the dynamics of the momentum exchange as well as the effect of ionization and recombination, severely limiting the applicability of the model to the thruster plasma. Therefore, all the collision terms are retained in the electron momentum equations (10)-(12).

Equation (13) includes the effect of Joule heating, a contribution due to exchange of random thermal energy and due to ionization and recombination. The simulation of Katz et. al[15] shows that the average ion energy remains nearly constant in the channel. Therefore, we also assume in our model that the ion energy is constant.

In closure, equations (6)-(13) are supplemented with the simple form of Ohm's law,[35]

$$\mathbf{E}\equiv-\nabla\phi=\frac{m_ev_{ei}}{e}(V_i-V_e)+\left(\frac{1}{en_e}\right)\nabla n_iT_i \tag{14}$$

Equation (14) yields the relationship between the current and strength of the electric field in the plasma. The electric field has been written in the moving frame of the plasma, i.e. $\mathbf{E}\equiv\mathbf{E}'+\mathbf{V}\times\mathbf{B}$.

Before numerically solving the above set of equations (6)-(14), we normalize the physical variables as follows. Temperature T is normalized using the first ionization potential of Xenon, $T_* = E_i = 12.1$ eV. All other dependent variables can be normalized from:

$$V_* = \sqrt{\frac{T_*}{m_i}} = 2 \times 10^3 \text{ m/s}; \quad n_* = \frac{\Gamma_*}{V_*} = 0.5 \times 10^{17} \text{m}^{-3}; \quad v_* = \sigma_* n_* V_* = \sigma_* \Gamma_* \square 2 \times 10^5 \text{ s}^{-1}$$

where $\sigma_* = \sigma_0 \sqrt{\frac{m_i}{m_e}}$. The fundamental length scale l_0 is defined in terms of characteristic velocity and collisional frequency, $l_0 = V_*/v_*$. The time scale is $t_0 = 1/v_*$.

In order to numerically solve the formulation (6)-(14), proper initial and boundary condition specifications are necessary to make the problem well posed. The axial velocities of electrons and ions are not fixed at the inlet. Under typical conditions, next to the anode, a plasma sheath (typical width ~ Debye length) forms and ions must flow into the sheath from the quasi-neutral region. The axial velocity is near zero close to anode and then begins to rise at the edge of the acceleration zone, reaching a maximum velocity beyond the exit.[22] Such flow behavior has also been observed in the classical nozzle problem, where flow changes smoothly from subsonic (in the narrow region) to supersonic flow in the divergent region. Therefore, a sonic point, where the flow velocity equals the characteristic speed of the medium, is always expected at the exit. We shall impose the "choked exit"[19] boundary condition for the ion axial velocity. Furthermore, axial electron flow will be assumed inward at the channel exit. We impose zero radial velocity for the electrons and ions at the inlet and leave it floating elsewhere. At the inlet, the plasma density is equated to the reference value. The neutral density at the inlet depends upon the mass flow rate. In the present calculation, the mass flow rate is ~ 6 mg s^{-1}, a value relevant to a thruster operating at 1.5 kW power level.[2,14] The corresponding neutral density is $n_n \sim 10^{18}$ m^{-3}. The homogeneous Neumann condition is imposed on the electrostatic potential at the inlet. Since at the cathode, the potential is zero, a vanishing potential is assumed at the outlet. For ion density, a homogeneous Neumann condition is assumed. At the upstream boundary (thruster inlet plane), we specify an electron temperature of $T_e = 5$ eV, that is close to the experimental data.[6,25]

In a typical Hall thruster experiment, the radial magnetic field is dominant compared to the axial field. The radial magnetic field decreases from a typical maximum of about 200 G near the channel exit to a much lower value (~30–40 G) near the anode, though higher values of radial magnetic fields (~ 350 G) have been utilized recently for P5-class of thrusters.[2] The presence of this radial magnetic field inhibits electron flow to the anode, and in the process considerably enhances the ionization due to electron impact. In the presence of a very strong radial magnetic field and in the absence of any collision, the axial electron current may be completely inhibited. Thus, the current is mainly carried by the ions $j_z \approx j_i$. Assuming a quasineutral ($n_i \approx n_e$) plasma, the Hall current per unit radius is

$$J_H \approx en_e \int_0^r \left(\frac{E}{B}\right) dr \approx en_e \phi_d / B \qquad (15)$$

where ϕ_d is the discharge potential. Note that the discharge potential is the sum of the column potential drop ϕ, the cathode fall potential, and the possible potential drop in the plasma region next to the exhaust and outside the cylinders. The corresponding Hall current density can be expressed as

$$j_H = en_e E / B \approx en_e E_z / B_r \qquad (15a)$$

For $j_i \approx en_e V_i$, we have

$$J_H \approx j_i \phi_d / BV_i \approx j_i \sqrt{\frac{m_i \phi_d}{2eB^2}} \qquad (16)$$

where the maximum ion velocity is $V_i=(2e\phi_d/m_i)^{1/2}$. Clearly, for a given magnetic field, $J_H/j_i \sim \sqrt{\phi_d}$ For an efficient operating system, current is carried by the ions and ions attain maximum velocity. Thus we shall anticipate that the ensuing potential distribution (and the resultant accelerating electric field) will be in the region of maximum magnetic field strength.

IIa. Plasma-Wall Interaction

The walls of the discharge chamber of a stationary plasma thruster (SPT) are commonly made of composite ceramic materials, namely, boron nitride and silicate oxide. Among many reasons limiting the efficiency and lifetime of a Hall thruster, the most critical is the wear of the surface layer of the ceramic walls. The wall erosion of the thruster occurs due to the plasma-wall interactions. The coaxial wall of a thruster develops the non-uniformities due to sputtering, re-deposition, cracking, etc. Further, sputtered material may contaminate the spacecraft surface and affect the working parameter optimization. Although the lifetime issues are critical to its design, many physical aspects in thruster plasma are yet to be understood. The lifetime of an on-board Hall thruster is expected to exceed several thousand hours. This complicates the experimental investigation and numerical prediction of the wall wear as several parameters come into play during the operational lifetime of the thruster. This results in the lack of reliable data on the sputtering yield under operational conditions.

If the ion impact energy is sufficiently large, the impact ions may cause severe sputtering of the target, which is an undesirable side effect. The dielectric walls, anode and hollow cathode walls may develop the non-uniformities due to sputtering, re-deposition, cracking, etc. Further, sputtered material may contaminate the plasma. This can significantly affect the performance of the HET. The erosion of the wall can take place due to the ion bombardment (classical erosion) as well as due to the near wall electric fields (anomalous erosion). Whereas, ion bombardment can give rise to small-scale prominences mostly across the incident ions, the "anomalous erosion" is manifested as a periodic structure oriented along the ion flux with a period of the order of electron Larmor radius[13], indicating, sputtering due to electrons. The difference between the sputtering caused by the atoms and ions interaction with the wall is small and thus, it is sufficient to study the ion induced sputtering of the wall. This ejection normally occurs when the lattice particle receives sufficient energy from the incoming particle to overcome the binding potential of the solid. The minimum bombarding energy needed for sputtering is called the threshold energy. Experiments[36-38] indicate that the sputtering yield does not depend on the angle of incident ions and it varies linearly with ion energy. Present report employs a 1D model described below to study the effect of sputtering and secondary emission on the acceleration process inside the channel. It is anticipated that the result will provide the basic insight of the underlying physics of the plasma-wall interaction.

Also, the secondary electron emission (SEE) is an important issue. Secondary electron emission is the emission of electrons from the wall due to the electron bombardment. A high-energy primary electron enters the solid and dissipates its energy. Some of this energy goes into the creation of excited electrons and some of these electrons called secondaries escape from the wall. The "intermediate" energy

electrons are responsible for the ejection of secondary from the wall.[13] Since the ions and electrons have opposite charge, the emitted secondary electrons are accelerated away from target in the same electric field that accelerates the ions towards the target. This leads to considerable power loss since part of the power goes into the electrons.[38-39] Understanding sheath dynamics is also important in electric propulsion devices. Wall effects can significantly alter the dielectric wall characteristics of Hall thrusters, while impact of high energy ions may deteriorate the performance of electrodes in MPD thrusters. The design of the future nuclear device must deal with the problem of sputtered wall material. Sputtered wall material, for example, may be ionized in the scrape-off layer and possibly transported into the core plasma, or may be redeposit immediately if the ionization occurs inside the sheath.

Most of the commonly used plasma confining materials have SEE coefficients near or above 0.9 at moderate plasma temperature. For example, boron (15 eV), carbon (12 eV), aluminum (47 eV) etc. have SEE which can reach up to 0.9.[40] The effect of the cold SEE on the sheath has shown to reduce the sheath potential significantly.[8] In fact the onset of space-charge saturation when the electric field is reversed near the wall surface, has been found to take place within the plasma sheath when SEE coefficient is ~ 0.9.[8] Earlier experimental studies of the effect of SEE on plasma sheath potential showed that the cold electron emission affect bulk plasma properties.[9,41]

The thruster plasma is partially ionized gas, consisting of electrons, ions and neutral xenon particles. In such partially ionized plasma, elastic and inelastic process takes place simultaneously. The elastic collision involves only exchange of momentum and energy between colliding particles whereas inelastic processes like ionization, recombination, charge-exchange collision, plasma-wall interaction, secondary emission, sputtering etc. can be responsible for redistributing the number density of the particles along with its momentum and energy. Not all processes are equally probable. We describe the processes important for the channel dynamics besides ionization and recombination.

(a) Electron-ion and plasma-neutral collisions: Because of the long-range nature of the Coulomb force, plasma particles can be deflected over the Debye length λ_D. The electron-ion collision frequency is

$$\nu_{ei} = \frac{4\sqrt{2\pi}}{3\sqrt{m_e}} \frac{e^4 n_i L_e}{T_e^{3/2}} = \frac{L_e}{3\sqrt{2\pi}} \left(\frac{n_i}{n_e}\right) \left(\frac{\omega_{pe}}{n_e \lambda_{De}^3}\right) \quad (17)$$

Here, $\omega_{pe}^2 = 4\pi n_e e^2 / m_e$ is the square of the electron plasma frequency with an electron mass m_e and charge e, $\lambda_{De}^2 = T_e/(4\pi n_e e^2)$ is the square of the Debye length. $L_e = \ln(\Lambda)$ is the Coulomb logarithm. It has a typical value around 10 to 20. The plasma-neutral collision frequency is $\nu_{en} = n_n <\sigma V_{the}>$. For typical conditions of a Hall thruster, the effect of Coulomb collision (ν_{ei}) may be smaller or of the same order in comparison with the plasma-neutral collision (ν_{en}).[13,40]

(b) Plasma-wall interactions: The inelastic electron collision with the wall allows the electrons to move across the magnetic field toward the anode, giving rise to "near wall conductivity'. Thus, for modeling the near wall conductivity, one needs to specify the secondary emission and sheath potential The wall with high secondary electron emission δ can give rise to high cross-field conductivity, since a large

fraction of the incident energetic electrons are returned to the plasma as cold electrons with new guiding center drift along the direction of the electric field.

The modeling of the sputtering yield Y and isolating its effect on the performance of the thruster is complicated by the fact that as the plasma energy varies along the channel, close to the inlet, wall may not sputter at all whereas, near the exit, sputtering yield may be considerable implying that only a fraction of the accelerated ions across the channel strike the wall. Based on the experimental observations, we shall use an empirical formula used for sputter yield[42-43],

$$Y = \frac{S}{H_s}\left(E_i - 4H_s\right),$$ (18)

where $S = 1 \times 10^{-2}$ is the sputtering yield factor[37], $H_s = 3000$ K is the sublimation energy of boron nitride and E_i is the incident ion energy on the target. In the present work, we shall assume $E_i = 0.1\ T_e$. For a near wall sheath potential,

$$\varphi' = -\left[0.5 + \ln\left\{\frac{(1-\delta)}{(1-Y)}\left(\frac{m_i}{2\pi m_e}\right)^{1/2}\right\}\right]$$ (19)

electron-wall collision frequency, for a channel of width h can be given as,

$$\nu_w = \begin{cases} \dfrac{2V_{the}}{h}e^{\varphi'} & ; \varphi' \le 0, \\[2ex] \dfrac{2V_{the}}{h} & ; \varphi' \ge 0. \end{cases}$$ (20)

Here $\varphi' \equiv e\,\varphi/T_e$ and coefficient of secondary emission for Boron nitride wall is given as,

$$\delta = 0.198 \times T_e^{0.576}.$$ (21)

Owing to small inertia, electron response time is much faster than the ion response time. As a result, electron will attain steady state much faster than ions. Keeping this in mind, electron momentum and energy equations are solved as steady state equations, whereas for ions and neutrals, a set of time independent continuity and momentum equations are simultaneously solved. The axisymmetric cylindrical thruster plasma is modeled by 1D geometry where z corresponds to axial direction and θ is along the azimuth. Following one-dimensional equations are solved in the present work.[43]
Electron momentum equation:

$$V_{ez}\frac{\partial V_{ez}}{\partial z} = -\frac{1}{m_e n_e}\frac{\partial}{\partial z}(p_e) - \frac{e}{m_e}E_z - \left(\frac{\omega_c^2}{\nu_{ei}+\nu_{en}+\alpha_B\omega_c}\right)V_{ez} - \nu_{ei}(V_{ez}-V_{iz}) - \nu_{en}(V_{ez}-V_{nz})$$
$$-\left(\frac{S}{n_e}\right)(V_{ez}-V_{nz}) + \nu_w V_{ez}.$$ (22)

where m_e is the electron mass, n_e is the electron number density. V_{ez}, V_{iz}, V_{nz} are respective electron, ion and neutral axial velocities. $V_\theta = E_z/B_r$ is the azimuthal electron drift velocity, $p_e = n_e\,T_e$ is the electron pressure with T_e as electron temperature in eV, E_z is the axial electric field, $\omega_c = eB/m_e$ is the

11

electron-cyclotron frequency, and the source term due to ionization, recombination and charge exchange is $S = S_{recomb} + S_{ioniz} + S_{cex}$. Following relation between azimuthal and axial velocities is utilized,

$$V_{e\theta} = \left(\frac{\omega_c}{V_{ei} + V_{en} + \alpha_B \omega_c} \right) V_{ez} = \Omega V_{ez}. \qquad (23)$$

where, α_B is the Bohm diffusion coefficient and Ω is the Hall parameter. Typical value of Hall parameter varies between $100 - 1000$.

We note that the suppression of axial electron mobility is due to the imposed radial magnetic field. The ion mobility remains unaffected by such a field. This allows plasma to support an electric field with a potential difference close to the applied voltage. Thus, we shall use equation (22) to determine the plasma potential inside the thruster. The dynamics of the electron is determined by the pressure gradient, by the electric and magnetic forces and by collisional exchange of momentum in equation (22). In the regions of sharp flow gradients, the effect of convective term may become finite and therefore, the convective term is retained in this formulation. Similarly, since collision time scales are much larger than the electron-cyclotron gyration time scale, one may ignore elastic and inelastic collision terms in comparison with the Lorentz force term $V \times B$ in the momentum equation. Such an approach, will exclude the dynamics of momentum exchange as well as the effect of ionization and recombination, severely limiting the applicability of the model to the thruster plasma. Furthermore, in addition to the presence of electron-ion and electron-neutral collisions, electron-wall collision is thought to play an important role in the electron transport.[13]

It is known that the classical short-range, binary collision between plasma particles v_{ei} and plasma-neutrals v_{en} are not sufficient to explain the cross field transport of the electrons and either by invoking Bohm diffusion[19] or by invoking plasma side-wall interaction,[13,40] such a behavior is explained. We model plasma wall interaction by introducing electron-wall collision frequency v_w. Further, the effect of anomalous Bohm conductivity have been included qualitatively by including the equivalent frequency $v_B = \alpha_B \omega_c$, that incorporates the effect of magnetic field fluctuations.

Neglecting the effect of radiation, viscous dissipation and thermal conduction, electron energy equation can be written as[43]

$$\frac{d}{dz} \left[n_e V_{ez} \left\{ \frac{m_e (1 + \Omega^2) V_{ez}^2}{2} + \frac{5}{2} T_e \right\} \right] - n_e e V_{ez} \frac{d\varphi}{dz} = 3 \frac{m_e}{m_i} n_e v_{ei} (T_i - T_e) + 3 \frac{m_e}{m_n} n_e v_{en} (T_n - T_e)$$
$$+ S \left(\frac{3}{2} T_e + \alpha E_I \right) - n_e v_w E^{'} \qquad (24)$$

Here T_e, T_i and T_n (~.3 eV) are electron, ion and neutral temperatures in eV, respectively, and E_I is the ionization energy of the Xenon. Equation (24) includes the effect of Joule heating, contribution due to the exchange of random thermal energy and due to the ionization and recombination and interaction of the plasma with the wall. The convective flux of kinetic energy includes the flux of azimuthal electron kinetic energy $V^2 = V_{ez}^2 + V_{e\theta}^2$. The value of α is between (2 –3).[19]

Ion continuity equation is[43]

12

$$\frac{\partial n_i}{\partial t}+\frac{\partial (n_i V_{iz})}{\partial z}=S-\ v_w n_i. \tag{25}$$

In ion momentum, the momentum exchange due to collision with electrons will not be significant as ion mean free path is generally larger (~0.3 m) than the size of the thruster (~.02 m). Also, we consider ions as unmagnetized, since the gyration radius of ions is typically large for a 200G field with an ion velocity 4×10^3 m/s. Thus we ignore the effect of magnetic field on the ion transport. The pressure term in ion momentum equation can be ignored as the thermal energy of the ion is much smaller than their kinetic energy i.e. $T_i\!<\!<\!m_i V_i^2$. Then ion momentum becomes,[43]

$$\frac{\partial V_{iz}}{\partial t}+V_{iz}\frac{\partial V_{iz}}{\partial z}=\left(\frac{e}{m_i}\right)E_z+\left(\frac{m_e}{m_i}\right)v_{ei}(V_{ez}-V_{iz})-\left(\frac{m_n}{m_i}\right)v_{in}(V_{iz}-V_{nz})-\left(\frac{S}{n_e}\right)(V_{iz}-V_{nz})+v_w V_{iz}. \tag{26}$$

Neutral continuity: $\dfrac{\partial n_n}{\partial t}+\dfrac{\partial (n_n V_{nz})}{\partial z}=-S_n. \tag{27}$

Equations (22)-(27) are supplemented with the current and mass conservation equations respectively as

$$en_i(V_{iz}-V_{ez})=J_T \tag{28}$$

$$m_n n_n V_{nz}+m_i n_i V_{iz}=\frac{\dot{m}}{A} \tag{29}$$

Here $J_T = I_d/A$ is the total current density; I_d is the total discharge current, A is the cross section of the thruster channel and $\dot{m}$ is the mass flow rate.

Before numerically solving above set of basic equations, the physical variables are normalized using experimental data. The mass flow rate of the propellant is $\dot{m}=\rho VA$. Then the flux of the propellant is Γ $= 10^{23}$ m^{-2} s^{-1}. Temperature T_e is normalized to first ionization potential of Xenon, $T_* = E_i$ (12.1 eV). Then all dependent variable can be normalized from $V_* = \sqrt{(T_*/m_i)}$ m/s, $n_*= \Gamma_*/V_*$ m^{-3}, $v_* = \sigma_* \Gamma_*$ s^{-1} where $\sigma_* = \sigma_0 \sqrt{(m_i/m_e)}$, $\sigma_0 \cong 3.6\times 10^{-20}$ m^2 for Xe. The fundamental length scale can be defined in terms of characteristic velocity and collisional frequency as, $l_0 = V_*/v_*$. The time scale is $t_0 = v_*^{-1}$.

III. Improved Numerical Modeling

Finite element (FE) techniques are well known for their adaptability to arbitrary multidimensional geometries and accurate imposition of complicated boundary conditions.[44-47] Here, a multi-dimensional finite element formulation will be employed to solve charge-neutral continuity, momentum and potential equations. These equations may be expressed as $L(U)=0$, where U contains all state variables, e.g., ion density, ion velocity, potential, and L is a differential operator. The weak statement associated with a variational integral underlines the development of this numerical algorithm. The physical domain is spatially semi-discretized (^{h} approximated) using generic computational domain, i.e., the finite element. The state variables are interpolated inside the element, via the trial space FE basis set $N_k(x_j)$ that typically contains Chebyshev, Lagrange or Hermite interpolation polynomials complete to degree k and

to dimension j. The spatially semi-discrete FE implementation of the *weak statement* WS^h for $L(U)=0$ leads to

$$WS^h = S_e \left(\int_{\Omega_e} N_k L_e(U) d\tau \right) \equiv 0 \tag{30a}$$

$$= S_e \left(\int_{\Omega_e} N_k \frac{dU}{dt} + \int_{\Omega_e} N_k (s) d\tau + \int_{\Omega_e} \frac{\partial N_k}{\partial x_j} \left(f_j - f_j^v \right)_e d\tau - \oiint_{\partial\Omega_e \cap \partial\Omega^h} N_k \left(f_j - f_j^v \right)_e \hat{n}_j d\sigma \right) \tag{30b}$$

S_e symbolizes the "assembly operator" carrying local (element e) matrix coefficients into the global arrays, s is a source term (e.g. inelastic processes) and f_j and f_j^v are convective and dissipative flux vectors, respectively, and $\hat{n}$ is the direction normal. Application of Green-Gauss divergence theorem "weakens" the order of derivatives in (30a) and yields natural homogenous Neumann boundary conditions. The surface integral in the second line (30b) contains the (un)known boundary fluxes wherever fixed or flux boundary conditions are enforced accurately.

Independent of the physical dimension of the working domain Ω, and for general forms of the flux vectors, the semi-discretized weak statement always yields an ordinary differential equation (ODE) system that is *fully discretised* using a θ-implicit or τ-step Runge-Kutta type time integration. The terminal ODE is usually solved using a Newton-Raphson scheme for $U(t)$:[48-49]

$$U_{\tau+1}^{i+1} = U_{\tau+1}^i + \Delta U^i = U_\tau + \sum_{p=0}^{i} U^{p+1}, \text{ where } \Delta U^i = -[M + \theta\Delta t(\partial R / \partial U)]^{-1} R(U) \tag{31}$$

Here, a θ-implicit time marching procedure is employed. In (31), $M = S_e(M_e)$ is the "mass" matrix associated with element level interpolation, R carries the element convection, diffusion and source information. The calculation of the "Jacobian" $\partial R/\partial U$ and inversion of the $M+\theta\Delta t(\partial R/\partial U)$ matrix with sufficient accuracy is obviously a numerical challenge. However, unlike the traditional finite difference/volume methods, the present FE algorithm allows one to simulate the system simultaneously without requiring any sub-iteration for the Poisson solver.

The stiffness of the jacobian matrix for such coupled nonlinear problem becomes very high for realistic mass ratio of electron and ion. This results in solution divergence for standard finite difference/volume/element numerical approach on a moderate to fine mesh and require filtering and other expensive approaches for solution control. As a remedy, we utilized an efficient, high-order accurate, sub-grid embedded (SGM) finite element method[50-51] to achieve stable monotone solution on a relatively coarse mesh (see Figure 2). SGM elements utilize a non-linear sub-grid basis function, which is determined based on the local fluid velocity, mesh size and conductivity. SGM also serves as an excellent preconditioner for parallel solvers as it improves positive definiteness in the element matrix. Further details of the code are described in Ref. 44-46 and in Ref. 49.
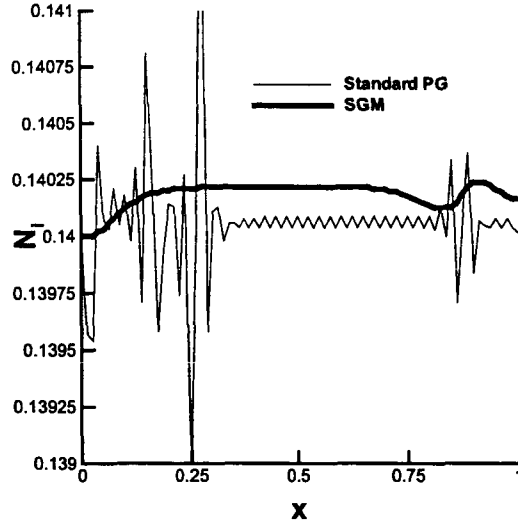
Figure 2. Coarse mesh comparison between standard Petrov-Galerkin and sub-grid embedded solutions for the ion number density distribution after 10^{-6} sec (from Ref. 44).

The choice of time step is dictated by the Courant-Fredrich-Lehy condition.[52] The solution at any time step is declared convergent when the maximum residual for each of the state variables becomes smaller than a chosen convergence criterion of $\epsilon=10^{-4}$. The steady state is declared when the above convergence criteria is met at the first iteration of any time step. Here, the convergence of a solution vector U on node j is defined as the norm:

$$\frac{\|U_j - U_{j-1}\|}{\|U_j\|} \leq \epsilon \qquad (32)$$

IV. Numerical Results and Discussion

We recall that the thruster plasma is modeled by a 2D axisymmetric (r-z) geometry, where r corresponds to the radial direction and z corresponds to the axial direction. The θ–direction is along the azimuth. We consider a two-dimensional magnetic field with radial and axial components, where the radial field is dominant (Fig. 3). The magnetic field lines near the exit close outside the thruster indicating that the near plume region plasma will be affected by the presence of the magnetic field. However, the simulation domain in the present work corresponds only to the bounded region. We have employed a trapezoidal time stepping procedure, i.e. $\vartheta=0.5$ in (31), for this model. In the present formulation the ion dynamics are time dependent, whereas electron dynamics have been assumed time-independent. This is a plausible assumption since, owing to their small inertia, the electron will reach a steady state over the ion dynamic scale.[10] The code uses variable time steps until the transient features die down and the iteration converges to a steady state. All solutions presented in this section have iterated to a steady state.
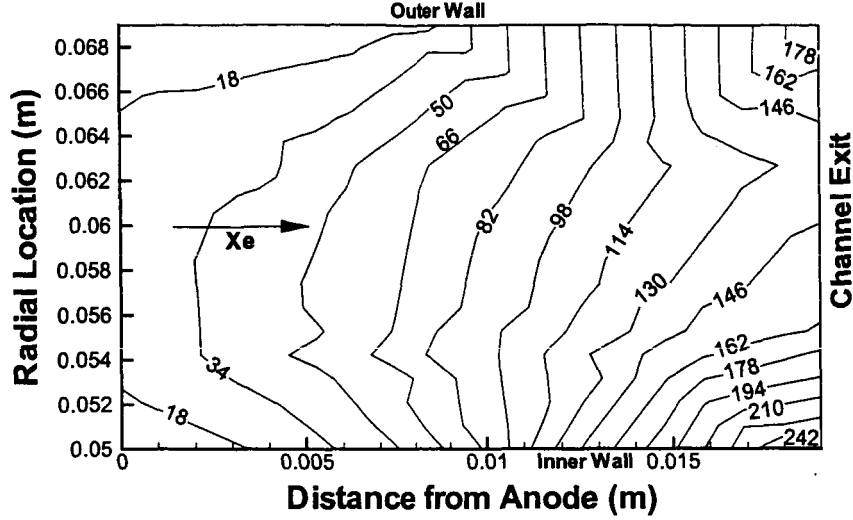
15

Figure 3. Measured radial magnetic field in Gauss inside the thruster acceleration channel.

Fig. 4a describes the neutral density contours. We use the reference values of physical parameters pertaining to a typical 1.5 kW class thruster that has a mass flow rate ~ 6 mg s^{-1} corresponding to n_n = 10^{18} m^{-3}. As is clear from the figure, neutral density is the highest at the inlet region and gradually decreases towards the channel exit. As ionization increases towards the exit (due to an increase in the electron temperature), the neutral number density should decrease and we see such a behavior. This is consistent with the fact that as a neutral enters the thruster chamber it undergoes impact ionization. Some experiment in the literature[10] suggests that the minimum in neutral density is not necessarily correlated to the corresponding increase of the ion density. However, in the present work the plasma density prediction displays a correlation between ion and neutral number densities that is similar to the reported experimental data.[2,6] We attribute this correlation to the temperature dependent, self-consistent calculation of the ionization rate.

Fig. 4b plots the plasma number density contours. The ion (electron) number density increases rapidly from a base value of 10^{17} m^{-3} and attains a maximum value 7×10^{17} m^{-3} upstream of the acceleration channel before decreasing near the exit. The experimental results[2,14] show that the plasma density reaches its peak value inside the acceleration channel, near the inner wall before the exit plane. In this region, the radial magnetic field is the maximum and thus a large number of electrons are inhibited from moving in the axial direction, resulting in a high probability of impact ionization and plasma production. The maximum plasma density inside the acceleration channel agrees with the fact that the ionization channel is well inside the thruster. There is no significant effect of ionization and recombination on the plasma number density. This could have been anticipated on the grounds that in a Hall thruster, where the pressure is low and ion currents exceed the electron current, the effect of the ion production and loss to the ion continuity equation (6) is negligible.[20]
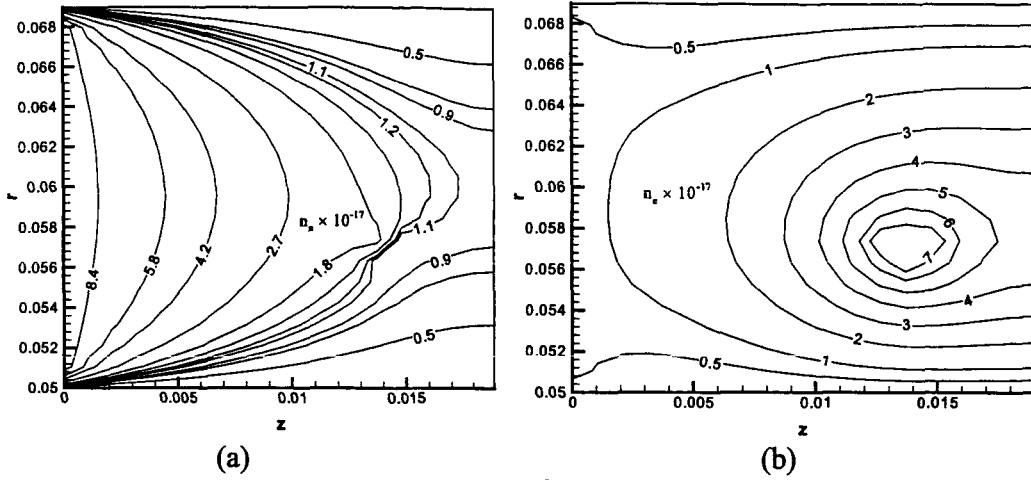
Figure 4. (a) Neutral number density contours in m^{-3}, (b) Plasma number density contours in m^{-3}.

The experimental result for a 1.6 kW class thruster[13] displays two distinct peaks in the ion number density profile located at about 0.02 m and 0.032 m from the anode. These peaks are attributed to different ionization mechanisms – to the electron thermal energy upstream (0.02 m) and to the availability of electron gyration energy at 0.032 m. These results underline the complexity of the thruster plasma dynamics and inadequacies of the existing numerical models. Several important questions need to be addressed in order to explain the physical mechanism behind the experimentally observed transition from double hump to single hump ion density profile when operating at 1.6 kW and 3 kW.[14] If at 1.6 kW, plasma undergoes a unique ionization-recombination-ionization cycle, then such behavior should be reflected in the neutral velocity and density profiles. We anticipate that at higher operating powers of the thruster, the neutral velocity will exhibit an initial increase (corresponding to the loss of slow neutrals due to ionization, i.e. number of fast neutrals increase), then decrease and again an increase. Also, the neutral number density should exhibit an initial decrease, then an increase and again a decrease in its number density. It points to the necessity of generalizing the numerical model on the one hand and further experimental investigation of the thruster plasma dynamics on the other hand.

The direction of ion streamlines as plotted in Figure 5 shows that the ion flow diverges towards the sidewalls in the downstream section of the channel, indicating the presence of a radial electric field. Haas[2] has experimentally inferred the presence of this radial field, where the radial asymmetry in the ion number density has been attributed to
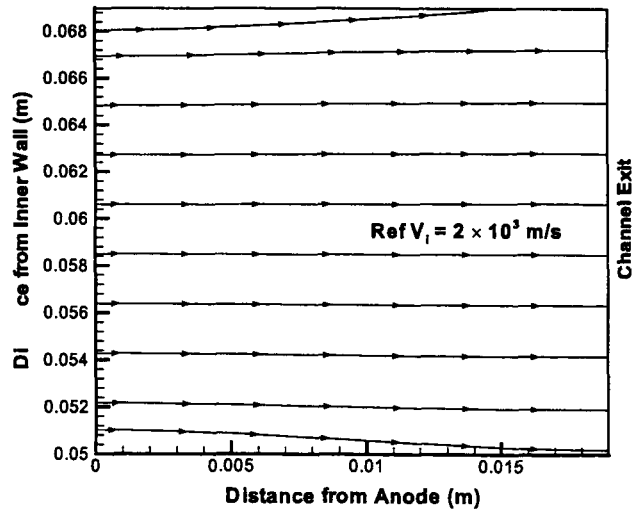

Figure 5. Directed ion trajectories show the decollimation of ions near the channel exit.

the presence of such a field. Figure 6 shows that the magnitude of the radial velocity contours increases in the region of strong magnetic field (B_r) confirming the experimental observation.[2] The interaction of ions with the ambient magnetic field could be another possible reason for divergence of the ion streamlines. The magnetic field, which confines the electrons in the azimuthal direction and inhibits their axial motion, may exert its influence on ions due to the collisional coupling of ions with the electrons – like ambipolar diffusion in the interstellar plasma.[53] Thus, even though ions are not directly coupled to the magnetic field, they may interact with the magnetic field through the electrons. We also anticipate that an additional divergence in the ion-beam may appear once the thermal pressure gradient is included in the ion dynamics. When the ion pressure gradient is taken into account, it will give rise to a radial electric field that may cause a dispersion of the accelerated beam. The decollimation of the ion beam in the radial direction will reduce the thrust.

In addition, in the presence of ionization and recombination there is a slight increase in the ion radial velocity near the exit as shown in Fig. 6. This increase in the radial velocity could be due to the depletion of the slow ions to the walls. However, a definite correlation between the

Figure 6. Radial velocity contours in m/s.

velocity and density can only be made if plasma-wall interactions are also included in the model. Recent numerical studies[21] suggest that plasma-wall interaction may affect the plasma density, near the exit plane.

Figure 7 describes the electron temperature contours. We note that the increase in the temperature is not uniform in the channel. The maximum increase of ~28 eV occurs just downstream of the center of channel, towards the inner wall. The peak in the temperature can be attributed to the Ohmic heating due to the maximum gyration energy in this region. The rise in temperature is similar to the measured electron temperature near the exit of the 1.6-kW class thruster of Hass and Gallimore.[14] However, the experimental electron temperature peak is spread along a radial line concentrated near the channel exit. Our numerical electron temperature results do not clearly reproduce this profile and may point to the limitation of the present model. Secondary electron

Figure 7. Electron energy distribution in eV.

emission, ion sputter yield, the electron near wall conductivity, the near wall sheath effect etc., may all

18

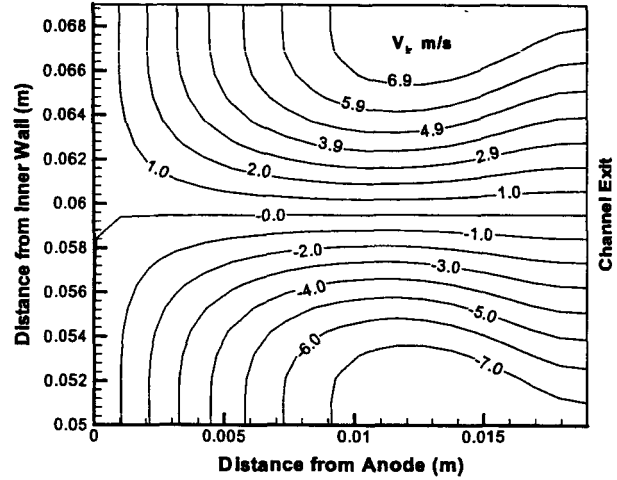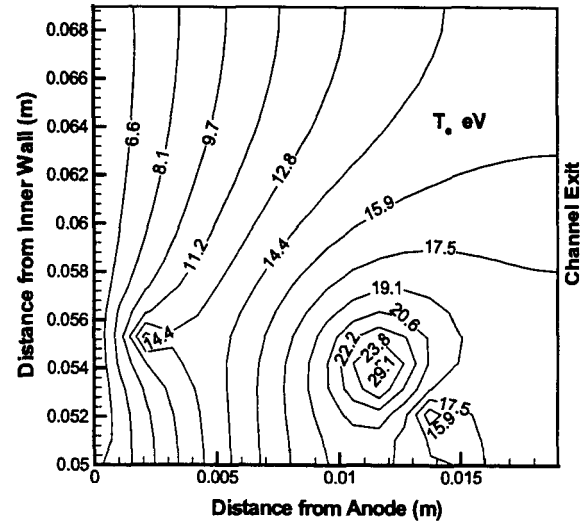affect the electron temperature profile. The present model will be extended to include plasma-wall interactions for better benchmarking with the experimental data.
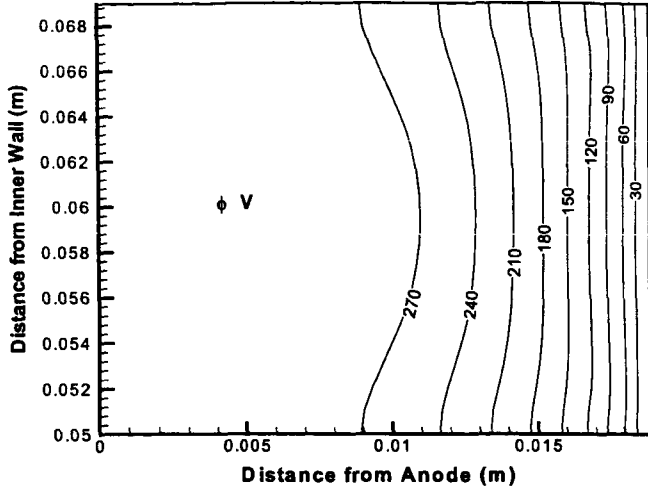

Figure 8. Potential distribution inside the acceleration channel in volts.

Figure 8 shows the potential contours inside the acceleration channel. The potential is highest at the inlet (near the anode) and is set to zero at the outlet (near the cathode). This is similar to the numerical approach presented by Haas.[2] Although the computed potential is set to zero at the channel exit, observations[2,14,17] indicate that only one half to one third of the potential drop actually takes place downstream of the thruster. In this numerical model, the full potential drop is forced to occur inside the channel. We further note that the potential inside the channel is very sensitive to the boundary conditions on the plasma velocities. Such effects will be evaluated in more detail if future support is available.

In Figure 9, the plasma number density, electron temperature, plasma potential along with the electric field and electron gyration energy are given at radial cross section $r = 0.056$ m, centrally located between the outer and the inner wall. We see that the plasma number density exhibits a narrow half width at full maximum (hwfm) just upstream of $z = 0.1$ m, suggesting a localized ionization region. It was noted by Kim[5] in one of the early experiments on SPT that a very small ionization region precedes the acceleration zone. Our numerical result is consistent with the experimental observations.[2,5] The electron temperature T_e profile in Fig. 9 predicts a sharp increase near the inlet and then a gradual rise before reaching the maximum of about 22 eV near the two-third length downstream of the channel. This is not consistent with the trend in plasma density profile. One would expect that the plasma density maximum will coincide with the electron temperature maximum, and that the first local maximum in electron temperature at around 14 eV at normalized axial location of 0.11 will be reflected in a small peak in the plasma density. However, the first local maximum in the temperature may reflect the loss of slow electrons due to recombination, since plasma number density is not a sensitive function of source or sink term[20], the local electron temperature maximum of 14 eV (at $z/L = 0.11$) does not affect the plasma density profile.
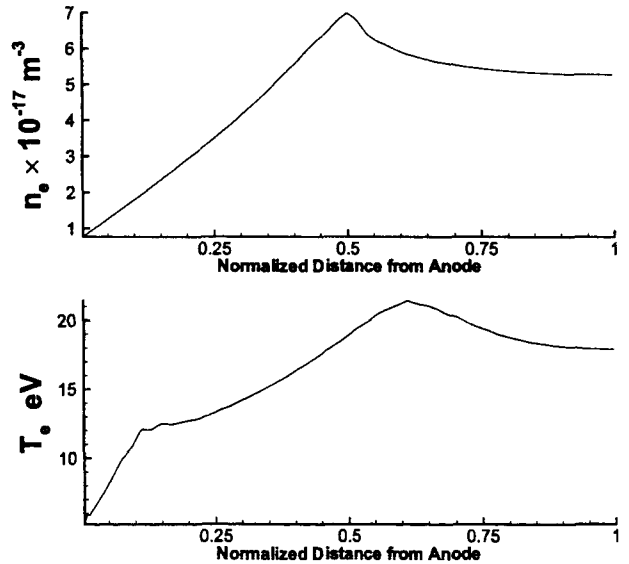

Figure 9. The distribution of electron density, and temperature below the centerline.

The computed potential profile is consistent with the known experimental data (with uncertainty of –3V/+6V) for a 1.5 kW thruster that operated at 300 V.[16] The potential profile is flat in most of the channel and approaches zero at the exit. Since potential is forced to zero at the exit, the simulation result starts diverging with the experimental result near the exit. The gyration energy (last frame in Fig. 9), displays an increasing trend, reaching maximum near the exit, which agrees well with the published Hall contours[2,21] that display a maxima upstream of the channel exit for 1.6 and 3 kW-class thrusters. Finally, the thrust at the exit plane of the thruster acceleration channel is calculated via Eqn. (24) of Haas and Gallimore.[54] The simulation result shows a steady state thrust of 79.4 mN, which is within the measured data of 95 3 mN and the calculated value of 68 mN at the exit plane of the 1.6 kW thruster.[54]
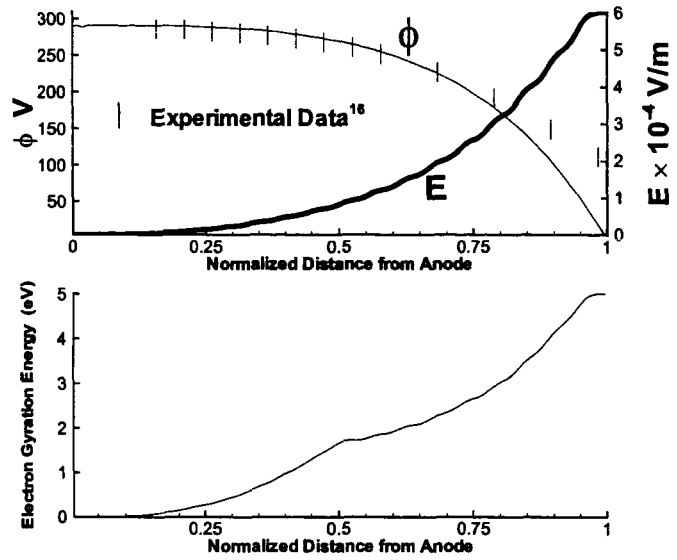

Figure 9 (cont.). The distribution of potential and electron gyration energy below the centerline (r=0.056m) of the acceleration channel.

In Figs. 10-13, the solutions of (22)-(29) are also documented to show the effect of sputter and SEE. The applied magnetic field has a peak upstream of the exit plane. The dotted line correspond to a case when only effect of secondary emission is considered in the plasma-wall interaction and bold line correspond to a case when both secondary emission and sputtering yield effect have been considered. The plasma number density (Fig. 10a) increases rapidly from a base value of 2.8×10^{17} m^{-3} and reaches a maximum value 1.6×10^{18} m^{-3} upstream of the acceleration channel before decreasing near the exit in the presence of secondary emission. However, when both secondary emission and sputter yield, due to ion-wall interaction are included, the decrease in number density is more pronounced toward the exit (bold line). The change in plasma density toward the exit in the presence of sputtering yield is consistent with the fact that plasma is partly lost to the wall and the effect is more pronounced near the exit of the channel. The experimental results[19] shows that the plasma density reaches its peak value inside the acceleration channel, right bottom corner of the exit plane. The location of ionization zone (~0.6) is same for both the cases. The maximum plasma density inside the acceleration channel is in agreement with the fact that the ionization channel is well inside the thruster.

The rapid increase in the ion number density is reflected in the rapid decrease in the neutral number density (Fig. 10b) from 2×10^{18} m^{-3} to approximately 1.6×10^{18} m^{-3}. This is consistent with the fact that as neutral enters the thruster chamber it undergoes the impact ionization. The effect of sputter yield and secondary emission (bold line, Fig. 10) is not very significant in comparison with the case when only secondary emission is present (dotted line).
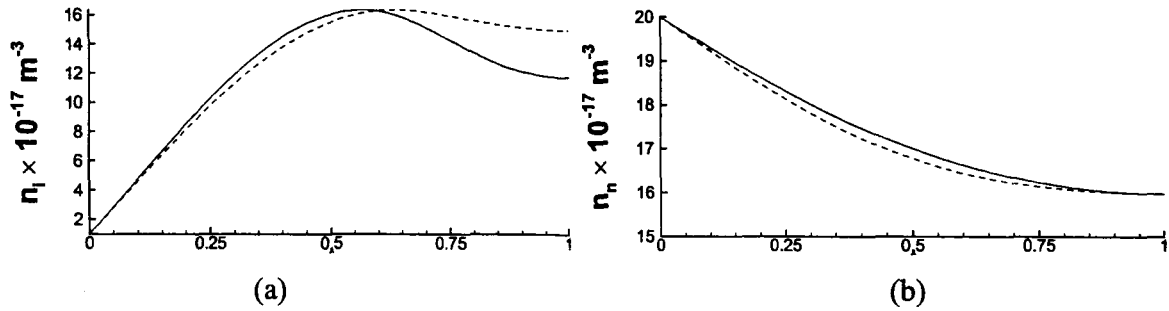
Figure 10. Effect of SEE and sputter yield on (a) ion and (b) neutral number densities.

Fig. 11a describes the axial ion velocity profile. The velocity peaks downstream of the channel, before the exit. This indicates that the location of the acceleration channel is inside the acceleration channel at 0.75. The ion velocity is slightly higher in the presence of sputtering (bold line) than in the presence of secondary emission only (dotted line) though difference is not very large. Ions are accelerated mainly due to the presence of the potential gradient, which is maximum near the channel exit, Fig. 6. Further, one may infer from the location of the acceleration channel that the width of the ionization region is narrower (~0.15) than the width of the acceleration channel (~0.25). This is in conformity with the experimental results.[6,25]

Fig. 11b shows the electron velocity profile. There is a slight increase in the electron velocity due to the slight increase in the electric field (Fig. 12, Bold line) in the presence of sputtering effect on the plasma-wall collision frequency. The electrons from the cathode, located just outside the chamber of a Hall thruster, are accelerated towards the anode. Large negative velocity near the exit is consistent with the large electric field, which are responsible for accelerating the electrons towards the inlet. These inward moving electrons, on their way to anode collide with the neutrals and ionize them. As a result, electron velocity decreases towards the anode as reflected in the figure.
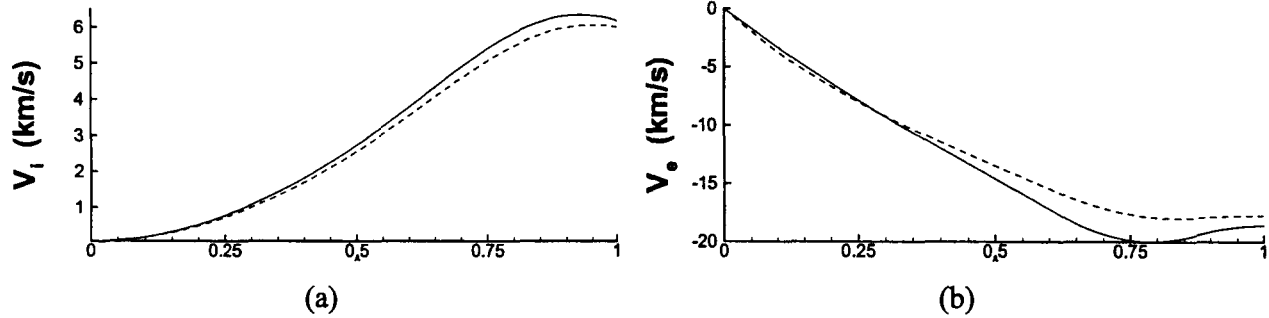

Figure 11. The effect of HET wall interactions on axial (a) ion and (b) electron velocities.

Figure 12 shows the potential profile inside the acceleration channel. The change in potential profile is not significant in two cases. We see that the potential has a zero gradient inside the thruster channel similar to the experimental data.[6] However, the computed potential vanishes at the channel exit, while observations[6,17] indicate that only one half to one third of the potential drop takes place downstream of

the thruster exit. This difference is due to the imposition of zero potential boundary condition at the exit plane in numerical simulation, i.e., full potential drop is forced to occur inside the channel.
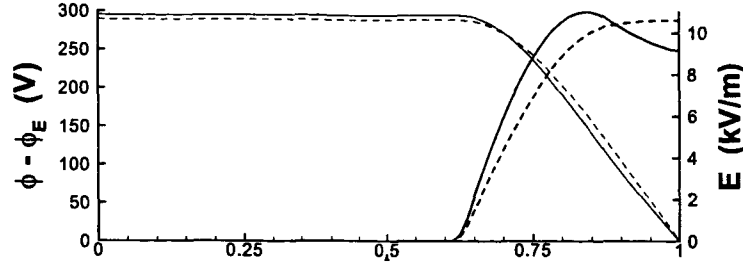
Figure 12. Electric field E and potential difference $\phi - \phi_E$. The potential remains unchanged for 2/3rd of the channel and then sharply drops to the exit potential ϕ_E.

In the presence of sputtering effect, azimuthal electron drift velocity (Fig. 13) profile towards the exit is quite different than when only secondary emission is present in the plasma-wall collision frequency. The azimuthal velocity $V_{e\theta}$ increase in the presence of sputtering yield is consistent with the electric field profile (Fig. 12 bold line). Towards the exit, $V_{e\theta}$ is smaller than in the absence of sputtering (dotted line). This behavior indicates that the plasma-wall interaction affects the potential towards the exit. This is consistent with the change in electric field profile in the previous figure. The drift velocity is a consequence of the crossed electric and magnetic field and gives rise to Hall current density, $J_H \approx e \, n_e \, V_\theta$. In Fig. 13, the peak in the azimuthal velocity considering sputter yield (bold line) is consistent with the electron temperature profile.
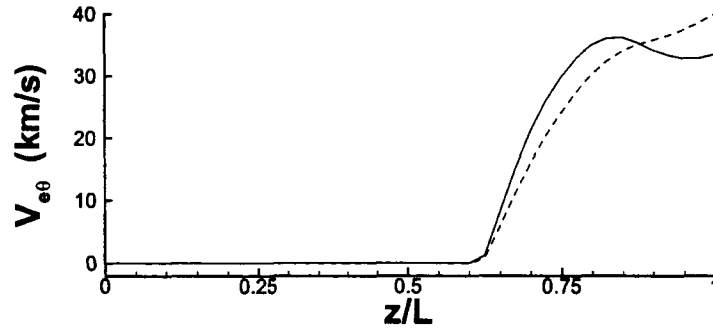
Figure 13. Electron drift velocity with sputter yield predicts the maximum just upstream of the channel exit (bold); the trend is different in the case without the sputter (dotted line) where the peak is at the exit plane.

The temperature distributions in two cases are not very different. The increase in the temperature is not uniform in the channel. The maximum increase occurs just downstream of the center of the channel in both cases. However, when plasma-wall interaction considers the ion sputter yield effect, electron temperature decreases slightly towards the exit (bold line). The peak in electron temperature can be attributed to the Ohmic heating due to the maximum gyration energy in this region. This trend in temperature distribution is similar to the results reported in the literature.[19] The computed temperature profile is in agreement with the measured electron temperature near the exit.[6,25]

Finally, the new NASA-457M (Fig. 14) is modeled and simulated for two flowrates and for two different fluids, namely, xenon and krypton at 464 sccm and 829 sccm. The 464 sccm case corresponds to an anode mass flow rate of 29.1 mg/s for krypton and 45.8 mg/s for xenon. The 829 sccm case corresponds to an anode mass flow rate of 52 mg/s for krypton and 86.4 mg/s for xenon. For a given proprietary magnetic field and a fixed channel (2.5"×2"), four cases are simulated by imposing a potential drop across the channel. Table 1 summarizes these results.
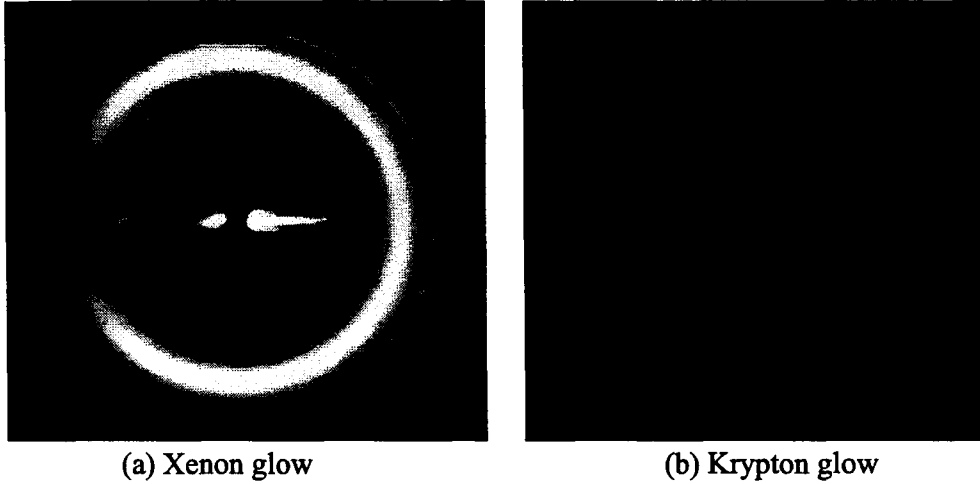

(a) Xenon glow   (b) Krypton glow

Figure 14. NASA-457M during testing.

Gas	Discharge Voltage (Volts)	Anode Massflow rate (mg/s)	Calculated Thrust (mN)	Specific Impulse (seconds)	Discharge Efficiency
Xenon	400	45.8	989.4	2201	59.2%
		86.4	1983	2240	61.3%
Krypton	400	29.1	703.2	2463	53.2%
		52.0	1335.1	2617	56.3%

Table 1. NASA-457M computed results.

V. Conclusions:

In this report, a finite element based multidimensional formulation of partially ionized plasma using multi-component fluid equation is developed in the presence of ionization, recombination and wall losses. The effect of inelastic processes viz. secondary emission and sputter yield has been incorporated. The model is then applied to study the dynamics inside the Hall thruster. The ion and neutral dynamics are time dependent, whereas electron dynamics is assumed time-independent. By using a third order electron temperature-dependent polynomial, a self-consistent calculation of the ionization rate has been carried out in the model. Our simulation results suggest that the increase in the plasma number density is correlated with the decrease in the neutral number density. The plasma density prediction is similar to

the reported experimental data.[2,5] There is no significant effect of the ionization and recombination on the plasma number density. This fact is consistent with reported observation[20].

The electron temperature inside the channel shows a gradual increase at the centerline, and predicts a hump upstream of the exit at a location between the centerline and the inner wall, which is in agreement with the experimental observation[2] that shows a peak next to the exit for a 1.5 kW class thruster. The potential profile agrees with recent experimental studies.[17] The ion streamlines suggests that ions are primarily accelerated due to the axial electric field and reach the maximum velocity near the exit plane. The ions are moving towards the sidewalls near the thruster exit, indicating the presence of a finite radial electric field. Experimental data[2] confirms the presence of such a radial electric field. The numerical results are very sensitive to boundary conditions. Therefore, boundary condition issues require a detailed investigation. Also, proper modeling of the plume region is necessary to make this model useful for design purposes.

Reference:
[1]V.V. Zurin, H.R. Kaufman and R.S. Robinson, "Physics of closed drift thrusters", Plasma Sources Sci. Tech., Vol. 8, p. R1-R20, 1999.

[2]J. M. Haas, "Low-perturbation interrogation of the internal and near field plasma structure of a Hall thruster using a high-speed probe positioning system", Ph.D. Dissertation, University of Michigan, 2001.

[3]D. Manzella, R. Jankovsky and R. Hofer, "Laboratory Model 50 kW Hall Thruster", 38th Joint Propulsion Conference, AIAA-2002-3676, 2002.

[4]E. Y. Choueiri, Phys. Plasma, "Plasma oscillations in Hall thruster", Vol.8, 2001, p.1411, 2001.

[5]R. Jankovsky, S. Tverdokhlebov and D. Manzella, "High Specific Impulse Hall Thruster Technology", 35th Joint Propulsion Conf., AIAA-99-2949, 1999.

[6]A.M. Bishaev and V. Kim, "Local plasma properties in a Hall current accelerator with an extended acceleration zone, Soviet Physics, Technical Physics", Vol. 23, no. 9, pp. 1055-1057, 1978.

[7]V. Kim, J. Propulsion and Power,"Main Physical Features and Processes Determining the Performance of Stationary Plasma Thrusters", Vol. 14, p.736, 1997.

[8]K. Komurasaki and Y. Arakawa, Two-dimensional numerical model of plasma flow in a Hall Thruster, J. of Propulsion and Power, Vol. 11, pp. 1317-1323, 1995.

[9]J. M. Fife, Hybrid pic modeling and electrostatic probe survey of Hall thrusters, PhD thesis, MIT, 1998.

[10]J. P. Boeuf and L. Garigues, "Low frequency oscillations in a stationary plasma thrusters", J. of Applied Phys., Vol. 84, p. 3541, 1998.

[11]A. Fruchtman and N. Fisch, "Modeling of a Hall Thruster", AIAA-98-3500, 34th Joint Propulsion Conf., Cleveland, OH, 1998.

[12]G. Guerrini, and C. Michaut, "Characterization of high frequency oscillations in a small Hall-type thruster", Phys. Plasma, Vol. 6, p. 343, 1999.

[13]A.I. Morozov and V.V. Savelyev, "Fundamental of stationary plasma thruster theory", Reviews of Plasma Physics, Vol. 21, ed. B.B. Kadomtsev and V.D. Shafranov, Consultants Bureau, New York, p.261, 2000.

[14]J.M. Haas and A.D. Gallimore, "An Investigation of Internal Ion Number Density and Electron Temperature Profiles in a Laboratory-Model Hall Thruster", AIAA-2000-3422, 36th Joint Propulsion Conf. (JPC) Huntsville, AL, July 16-19, 2000.

[15]I. Katz, M. Mandell and Y. Mikellides, 1-D HET code, (Internal memo to D. Manzella), Maxwell Tech., 2000.

[16]A.A.Litvak and N.J.Fisch, "Resistive instabilities in Hall current plasma discharge", Phys. Plasma, Vol. 8, p. 648, 2001.

[17]J.M. Haas and A.D. Gallimore, Phys. Plasma, "Internal plasma potential profiles in a laboratory-model Hall thruster", Vol. 8, p. 652, 2001.

[18]A. Fruchtman, N. J. Fisch and Y. Raitses, "Control of the electric field profile in the Hall thruster", Phys. Plasmas, Vol. 8, p. 1048 , 2001.

[19]E. Ahedo, P. Martinez and M. Martinez-Sanchez, "One-dimensional model of the plasma flow in a Hall thruster", Phys. Plasmas, Vol. 8, p. 3058, 2001.

[20]E. Choueiri, "Fundamental difference between the two Hall thruster variants", Phys. Plasmas, Vol. 8, p.5052, 2001.

[21]M. Keidar, I.D. Boyd and I.I.Beilis, "Plasma flow and plasma-wall transition in Hall thruster channel", Phys. Plasmas, Vol. 8, p. 5315, 2001.

[22]T. B. Smith, D. A. Herman, A. D. Gallimore, and R. P. Drake, "Deconvolution of Axial Velocity Distributions from Hall Thruster LIF Spectra", IEPC-01-019, 27th International Electric Propulsion Conference, Pasadena,CA, October 15-19, 2001.

[23]S. Roy and B.P. Pandey, "Development of a Finite Element Based Hall Thruster Model", J. Propulsion and Power, Vol. 19, n5, p. 964-71, 2003.

[24]N. Gascon, N.B. Meezan and M.A. Cappelli, " Low Frequency Plasma Wave Dispersion and Propagation in Hall Thrusters", IEPC-01-56, Pasadena, California, 2001.

[25]W.A. Hargus Jr. and M.A. Cappelli, "Interior and Exterior Laser Induced Fluorescence and plasma measurements within a Hall thruster", J. Propulsion and Power, Vol. 18, pp. 159, 2002.

[26]E. Ahedo, J. M. Gallardo and M. Martinez-Sanchez, "Model of the plasma discharge in a Hall thruster with heat conduction", Phys. Plasmas, Vol. 9, 4061 (2002).

[27]S. Roy and B.P. Pandey, "Numerical investigation of a Hall thruster plasma", Phys. Plasmas, Vol 9, 4052 (2002).

[28]S. Roy and B.P. Pandey, "Plasma-wall interaction inside a Hall thruster", J. Plasma Phys., Vol. 68, 305 (2003).

[29]S. Roy and A.J. Baker, "A nonlinear, sub-grid embedded finite element basis for accurate monotone steady CFD solutions", Numerical Heat Transfer – Part B, vol. 31, no. 2, pp. 135-176, 1997.

[30]S. Roy and A.J. Baker, "A nonlinear, sub-grid embedded finite element basis for accurate monotone steady CFD solutions - Part II, Navier-Stokes solutions", Numerical Heat Transfer – Part B, Vol. 33, no. 1, pp. 5-36, 1998.

[31]M. Mitchner and C. H. Kruger, *Partially ionized Gases* (Wiley-Interscience, New York, 1973).

[32]F. S. Gulczinski III, "Examination of the structure and evolution of ion energy properties of a 5 kW class laboratory Hall effect thruster at various operational conditions", Ph.D. Dissertation, University of Michigan, 1999, p. 142.

[33]V. E. Golant, A. P. Zhilinsky and I. E. Sakharov, *Fundamentals of Plasma Physics,* John Wiley, p.66, 1977.

[34]S. Pullins, Y. Chiu, D. Levandier and R. Dressler, "Ion Dynamics in Hall Effect and Ion Thrusters: Xe^+ + Xe Symmetric Charge Transfer", *38th Aerospace Sciences Meeting and Exhibit, Reno, NV, 2000* (AIAA, Washington DC, 2000), AIAA-2000-0603.

[35]L. Spitzer, *Physics of Fully Ionized Gases,* Wiley Interscience, p.35, 1962.

[36]J. F. Cuderman and J. J. Brady, Surface Sci., **10**, 410 (1968).

[37]Y. Garnier, V. Viel, J.F.Roussel, D.Pagnon, L. Magne and M. Touzeau, IEPC-99-083, Electric propulsion rocket society, 1999.

[38]V. Kim, V. Kozlov, A. Semenov and I. Shkarban, IEPC-01-073, 27th International Electric Propulsion conference, Pasadena, Califonia, 2001.

[39]D. Manzella, in *Proceedings of 24th International Electric Propulsion Conference, Moscow, Russia, 1995* (The Electric Rocket Propulsion Society, Worthington, OH, 1995), Vol. 1, p. 277.

[40]J. P. Boeuf and L. Garrigues, J. of Applied Phys. **84**, 3541 (1998).

[41]I.D. Boyd, L. Garrigues, J. Koo and M. Keidar, *36th AIAA Joint Propulsion Conference, Huntsville, AL, 2000* (AIAA, Washington DC, 2000), AIAA-2000-3520.

[42]M. J. Barlow, Mon. Not. R. astr. Soc., **183**, 377 (1978).

[43]S. Roy and B.P. Pandey, Journal of Plasma Physics, **68** (4), 305 (2002).

[44]S. Roy, B.P. Pandey, J. Poggie and D. Gaitonde, Physics of Plasmas, **10**(6), 2578 (2003).

[45]S. Roy, R. Raju, H.F. Chuang, B. Kruden and M. Meyyappan, Journal of Applied Physics, **93** (9) p. 4870-4879 (2003).

[46]S. Roy and B.P. Pandey, Journal of Propulsion and Power, 19(5), 964 (2003).

[47]S.B. Cooper, B. Kruden, M. Meyyappan, R. Raju, and S. Roy, Nano Letters, **4** (2) p. 377-381 (2004).

[48]S. Roy, Combining Galerkin matrix perturbation with Taylor weak statement algorithms, Computer Methods in Applied Mechanics and Engineering, Vol. 184, pp. 87-98, 2000.

[49]D. Balagangadhar and S. Roy, Design sensitivity analysis and optimization of steady fluid-thermal systems, Computer Methods in Applied Mechanics and Engineering, Vol. 190, no. 42, pp. 5465-5479 (Erratum, vol. 191, no. 3-5, pp. 509-510), 2001.

[50]S. Roy and A.J. Baker, Numerical Heat Transfer – Part B, **33**, p. 5 (1998).

[51]S. Roy and A.J. Baker, Numerical Heat Transfer – Part B, **31**, p. 135 (1997).

[52]R.D. Richtmyer and K.W. Morton, *Difference Methods for Initial-Value Problems,* 2d ed, Interscience Publishers, Wiley, New York, 1967.

[53]L. Spitzer, *Physical processes in the interstellar medium,* John Wiley, New York, 1978.

[54]J.M. Haas and A.D. Gallimore, "An Investigation of Internal Ion Number Density and Electron Temperature Profiles in a Laboratory-Model Hall Thruster", AIAA-2001-3507, 37th Joint Propulsion Conf. (JPC) Huntsville, AL, July 8-11, 2001.